Structure-Mechanical Relationships in Polymorphs of an Organic Semiconductor (C4-NT3N)

03 May 2024

Structure-Mechanical Relationships in Polymorphs of

Organic Semiconductor (C4-NT3N)

AUTHOR NAMES: *Chiara Cappuccino,† Luca Catalano,§ Francesco Marin,† Ghada Dushaq,§ Gijo Raj,§ Mahmoud Rasras,§ Rachid Rezgui,§ Massimo Zambianchi,‡ Manuela Melucci,‡ Panče Naumov,§* Lucia Maini†**

AUTHOR ADDRESS: † Dipartimento di Chimica "G. Ciamician", via Selmi 2, Università di Bologna, 40126 Bologna, Italy

§ New York University Abu Dhabi, P.O. Box 129188, Abu Dhabi, United Arab Emirates

‡ Consiglio Nazionale delle Ricerche-Istituto per la Sintesi Organica e la Fotoreattivita, (CNR-ISOF), via P. Gobetti 101, 40129 Bologna, Italy

KEYWORDS: polymorph, organic semiconductor, mechanical properties, crystal structure

ABSTRACT

Understanding of polymorphism of organic semiconducting materials is the key to structural control of their electrical and mechanical properties. Motivated by the ambipolar n-type charge transport and

electroluminescence of thienopyrrolyldione end-capped oligothiophenes, here we studied the propensity of one representative to crystallize as different polymorphs which display distinctly different mechanically properties. The crystal structures of the two polymorphs (denoted 'α' and 'β') of the material, 2,2'-(2,2'-thiophene-5,5'-diyl)bis(5-butyl-5H-thieno[2,3-c]pyrrole-4,6)-dione (C4-NT3N), were determined. In the α phase, the molecules interact strongly by π-stacking, forming columns which are bonded via C—H---O and chalcogen bonds, and this packing is consistent with the elastic behaviour observed with the crystals. Instead, the β phase has the molecules aligned along their core forming layers. Whilst the molecules interact strongly within the layers, they are practically unbound between the layers. The presence of slip planes in this form explains the plastic deformation induced by applying a force perpendicular to the (001). The thermal behaviour and the enantiotropic relationship of the polymorphs are reported.

1. INTRODUCTION

One of the most important tasks in the design and preparation of novel materials, yet a very challenging one, is the ability to predict and to control specific properties in the solid state. This is normally attempted by varying the chemical nature of the molecule and/or by using different 3D arrangements of the molecules in the structure via polymorphism, since polymorphs can present remarkably different properties.[1–5] Specifically, in case of molecular semiconductors, polymorphism is usually associated with prominent differences in photophysical and charge-transport properties, since the HOMO and LUMO energies are significantly perturbed by the crystal packing.[6] Within this context, efforts have been made to improve the charge transport and optoelectronic properties by modifying the molecular packing, either via chemical variation of the molecules[7–11] or by controlling

the polymorphic outcome during deposition.[12–19] Comparatively less studies are available that correlate the impact of crystal packing with the mechanical behaviour of this class of materials.[20–22]

Typically, molecular crystals are fragile, tend to break during deformation, and do not display flexibility.[23] In some cases, it is possible to elicit (irreversible) plastic deformation in crystals, and this is often accompanied by increased amount of structural defects and occasionally by delamination. However, there is a growing number of authors reporting elastic behaviour of molecular crystals where the original shape of the crystal is recovered after the deformation.[24–26] This is an attractive feature for real-world applications and, in particular, for semiconductor materials, since elasticity is of fundamental relevance to the fabrication and operation of mechanically compliant elements, such as flexible electronics and optoelectronic devices.[27]

In the past years, we have been researching thienopyrrolyldione end-capped oligothiophenes, for simplicity hereafter referred to as thienoimides (TI), which display ambipolar charge transport with major n-type behaviour and many are also electro-luminescent.[28–31] This combination of properties turns these materials into potential candidates for field-effect transistors (OFETs)[19,28] and single-layer ambipolar light-emitting transistor devices (OLETs).[29,32] The possibility for variations in the basic chemical structure provides access to a large variety of TI-based oligothiophenes which can be obtained by changing the length and shape of the alkyl chains, by modifying the number of thiophene rings, or by inserting different bridges between them.[28,31] It is noteworthy that most of these solids are obtained as different polymorphs, depending on the recrystallization conditions or the deposition procedure,[19] but the polymorphism is also evident for different alkyl chain lengths, as it has been observed with odd- and even-number alkyl chains.[33] The polymorphs usually can be easily distinguished by the different crystal morphology and luminescence.[34] Although the mechanical properties are apparently very important for their application, however, they have not been explored yet.

To provide more insight into their mechanical behaviour, we focused on the molecule 2,2'-(2,2'-thiophene-5,5'-diyl)bis(5-butyl-5*H*-thieno[2,3-c]pyrrole-4,6)-dione) (hereafter abbreviated C4-NT3N), which has been studied as potential ambipolar material.[29] The material appears in two crystalline forms denoted as 'α phase' and 'β phase' which are easily distinguished by their colour: α phase appears as orange crystals while β phase appears as yellow crystals. The material was used to construct a Time Temperature Integrator (TTI) device,[35] however the properties of the two crystal forms were not explored in detail. Herein, we describe the intriguing and distinct mechanical behaviour of the two polymorphs of C4-NT3N: while crystals of the β phase undergo plastic deformation, those of the α phase show complete elastic recovery in response to bending, a feature that is very rarely encountered with crystalline organic semiconductors. We were also able to determine the crystal structures of both polymorphs and we correlated the mechanical differences to their different packing.
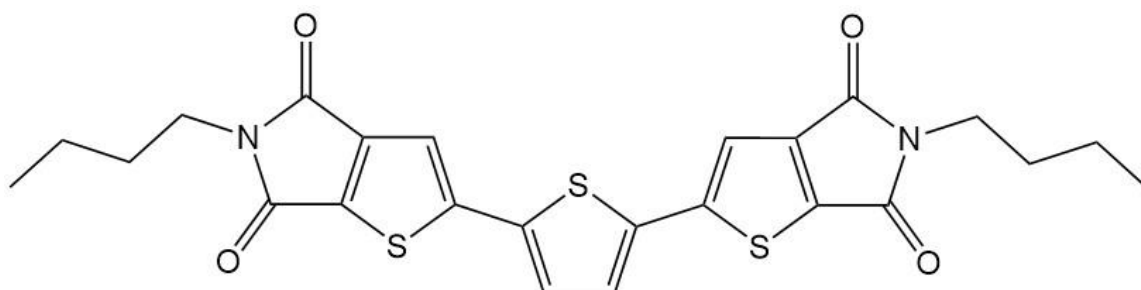

Chart 1. Molecular structure of the 2,2'-(2,2'-thiophene-5,5'-diyl)bis(5-butyl-5H-thieno[2,3-c]pyrrole-4,6)-dione (C4-NT3N).

2. RESULTS AND DISCUSSION

2.1. Polymorphism and crystal structure determination

The presence of different crystal phases was reported in the previous work of Gentili et al.,[35] but they did not assign the phase name, so hereafter the polymorphs are called α phase (Figure 1a) and β phase (Figure 1b).
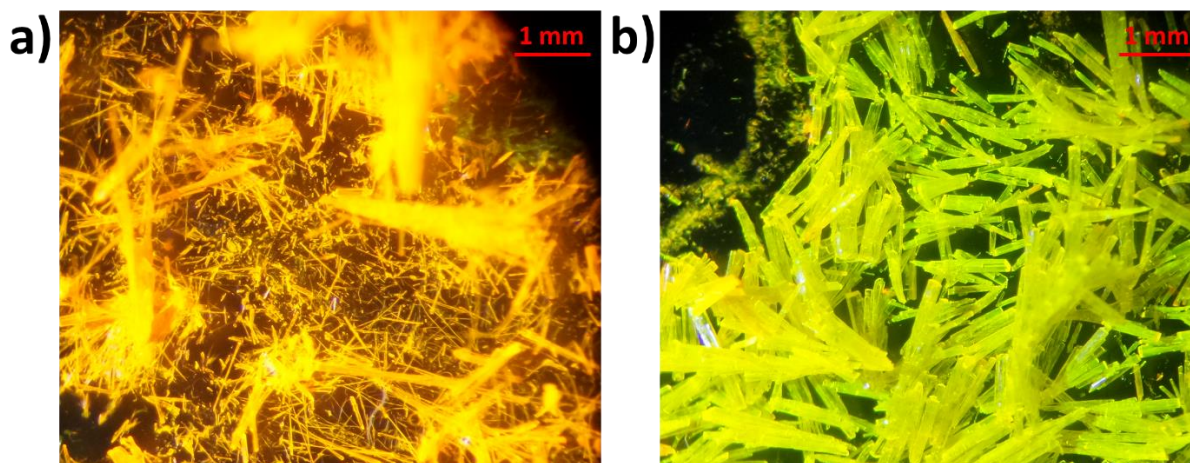

Figure 1. Appearance and emission of the crystals of the two polymorphs of C4-NT3N, the α phase (a), and the β phase (b). The images were recorded while the crystals were being irradiated with UV light (365 nm) at 30-fold magnification.

Crystals of the α phase suitable for single crystal X-ray diffraction (SCXRD) were obtained by solvent evaporation from a toluene solution. Plate-like crystals of the β phase, suitable for SCXRD, were obtained by slowly cooling a hot (100 °C) supersaturated solution of C4-NT3N in toluene or by using a solvothermal procedure. It was observed that usually the β phase crystallizes with some crystals from the α phase on the surface (see Supporting Information, SI, figure SI1). The structure of the α phase is triclinic, space group $P\bar{1}$, and cell parameters $a = 4.833(4)$ Å; $b = 11.579(6)$ Å; $c = 21.82(1)$ Å; $\alpha = 79.98(4)°$; $\beta = 89.87(6)°$; $\gamma = 83.60(5)°$; volume = 1194.8 Å^3), with one molecule in the asymmetric unit. The aromatic fragment is planar and the thiophene rings adopt an *anti-anti* conformation (Figure 2a) which allow the molecular core to assume a curved shape, while the alkyl chains are almost perpendicular to the thienoimide rings. The molecules are piled one above the

others, connected through π—π stacking interactions (Figure 2d). The main intermolecular interaction is in the direction of the columns which are formed by the molecules translated along the *a* axis (Figure 2c and 3). A secondary intermolecular interaction is due to the presence of C—H---O bond and chalcogen bond (S---O)[36] between two adjacent molecules, as suggested by the energy framework. The structure of the α form resembles that of the polymorph labelled form A observed for the similar molecule C4-NT4N.[33] The crystals grow along the [100] direction, and the visible faces are (010) and (001) (SI, Figure SI7).

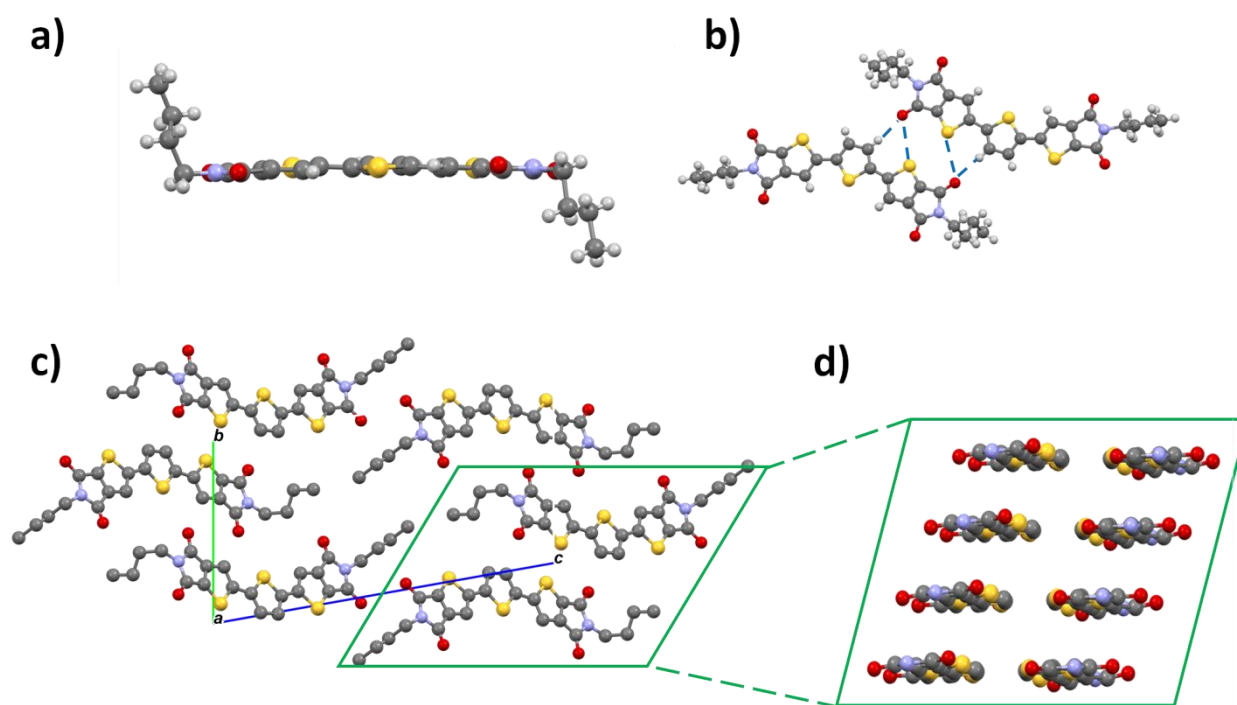**Figure 2.** Crystal structure of the α phase. (a) View of the molecular conformation; (b) Intermolecular interactions between the NT3N cores; (c) Packing viewed along the *a* axis showing the interdigitation of the columnar stacks of molecules; (d) π—π interaction among the molecules (the alkyl chains have been omitted for clarity). The hydrogen atoms have been omitted in panels c and d for clarity.
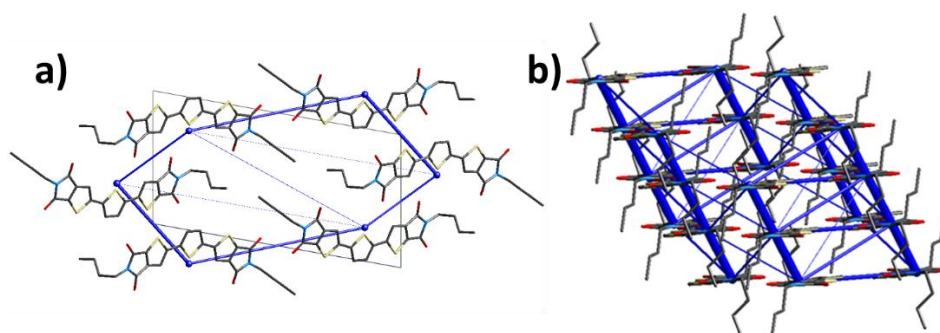
Figure 3. Graphic representation of the energy framework in the orange phase calculated with CystalExplorer[37–39]. The thickness of the line is directly correlated with the intensity of the interaction. (a) View along the *a* axis; (b) Details of the $\pi-\pi$ interactions.

The structure of the β phase was solved in the monoclinic space group $P2_1/c$, with one molecule of C4-NT3N in the asymmetric unit (a = 22.937(2) Å; b = 5.6167(4) Å; c = 19.323(1) Å; β = 104.806(8)°; volume = 2406.8 Å^3). The molecular core presents an internal disorder in the position of the sulphur atoms in one of the thienoimide groups. The disorder was modelled with 79% in the *syn* conformation (Figure 5a) and 21% in the *anti* conformation. Overlapped model of the C4-NT3N molecules in the α and β phases clearly shows that the molecules possess very similar conformations (Figure 4), however the molecule in *syn* conformation is less curved than the one in *anti* conformation. The crystal packing of β is similar to that of phase B of C4-NT4N.[32] The structure is wafer-like with layers where the molecules are strongly interconnected, as described by the 2D energy framework (Figures 6), and layers occupied only by alkyl chains that are almost free to move (as suggested by their high thermal parameters) and do not interdigitate with the upper layer of molecules. The crystals of the β phase are plate-like, and the morphology reflects the layered structure with preferred growth in the direction of the $\pi-\pi$ interactions (SI, Figure SI9) and expectedly, the shortest dimension corresponds to the long *a* axis.
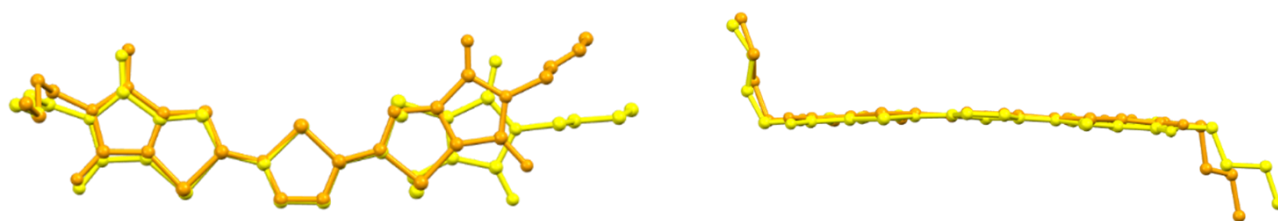
Figure 4. Overlap of the C4-NT3N molecules of the α and β polymorphs. The hydrogen atoms have been omitted for clarity.
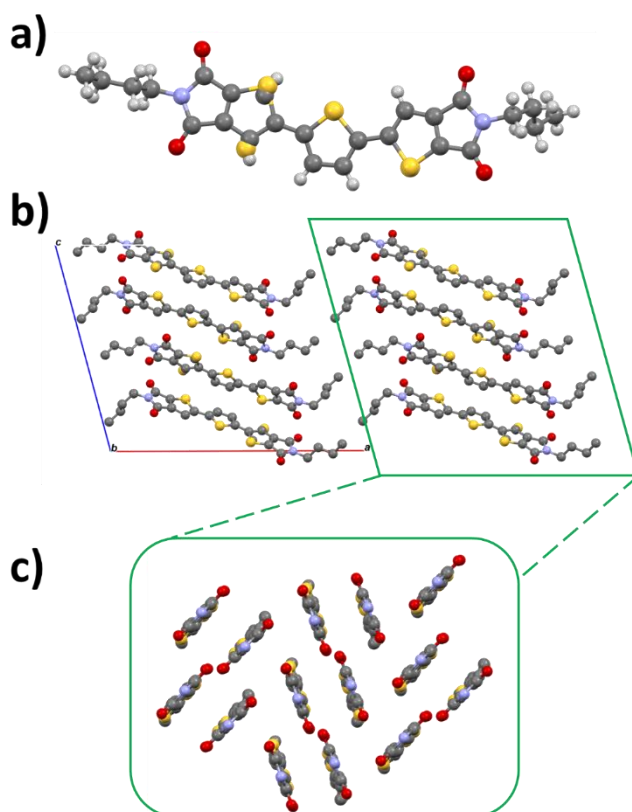
Figure 5. (a) View of the molecular conformation of the β phase; (b) View of the packing along the *b* axis, showing the organization of the molecules in layers; (c) π—π interactions between the

molecules from one molecular layer (the alkyl chains omitted). The hydrogen atoms in panels b and c have been omitted for clarity.
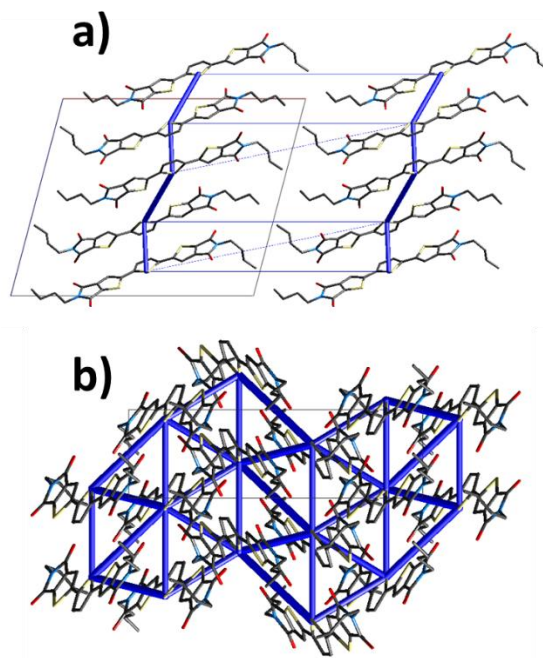
Figure 6. Graphic representation of the energy framework in the β phase calculated with CystalExplorer[37–39]. The thickness of the lines is directly correlated with the intensity of the interaction. (a) View along the *a* axis; (b) view along the *b* axis.

2.2. Thermal properties

The morphological changes that occur during the phase transition were investigated by using hot-stage microscopy (HSM) and differential scanning calorimetry (DSC). The DSC curve of the α phase shows two distinct events (SI, Figure SI4). The first one, at 205 °C with ΔH = 2.47 kJ/mol, is associated with transition to the β phase, as it was confirmed by variable temperature X-ray powder diffraction (VT XRPD) and in hot-stage microscopy (SI, figure SI2), while the second one, at 224 °C with ΔH = 35.5 kJ/mol, is relating to melting. On cooling the DSC shows two very close yet distinct

events. The first at 200 °C with ΔH = -2.36 kJ/mol correspond to a transition from the melt to a metastable liquid crystal phase that crystallizes at 199 °C with ΔH = -32.8 kJ/mol (second peak) as β phase. No solid-solid transition from β to α phase was observed during cooling.

The thermal behaviour was also monitored by HSM with a sample presenting both α and β phases. During heating α phase converts to the β phase above 205°C (Figure 7). By cooling, the liquid C4-N3TN forms liquid crystal, which can be easily detected at 201 °C (Figure 8a). Usually the transition from liquid crystal to crystal resulted in formation of β phase only, however the presence of impurities was found to induce concomitant crystallization of the two polymorphs (Figure 8c). Together with the DSC results, these results suggest that α crystals are the stable phase at room temperature, while the β crystals are the stable form at high temperature.
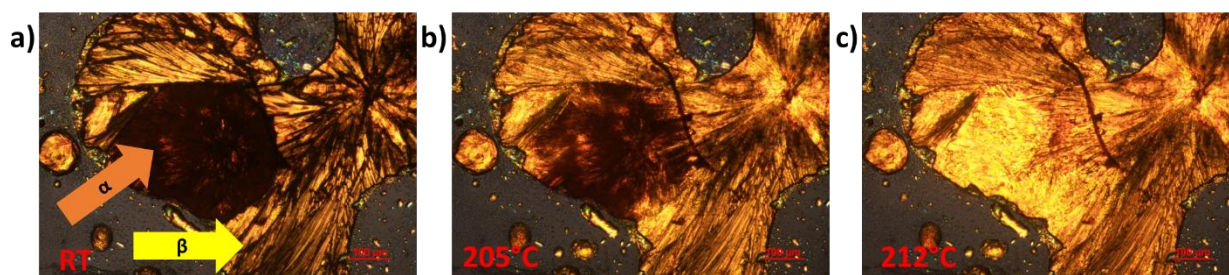

Figure 7. Hot-stage microscopy of a sample with both α and β phases. The transition of the α crystals to the β form is visible between 205 and 212 °C.
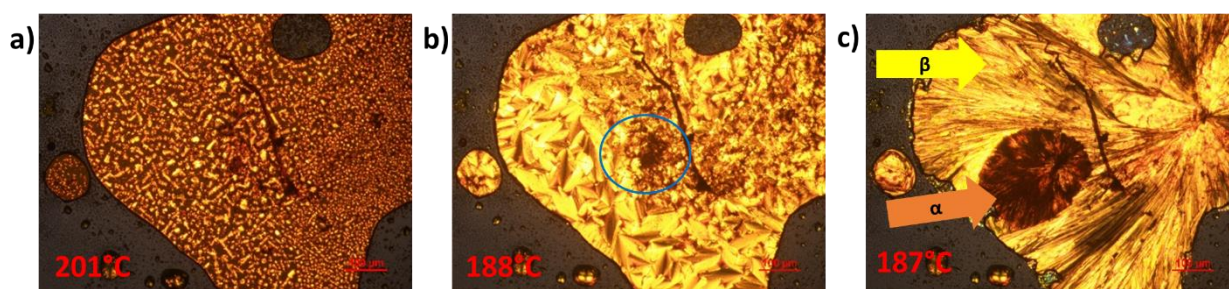

Figure 8. Hot-stage microscopy of a melted sample of C4-NT3N during cooling. (a) Onset of the

transition from melt to liquid crystal; (b) Onset of the transition from a liquid crystal to solid, in the blue circle the impurity which promotes α crystallization; (c) Crystallization of the two concomitant polymorphs.

2.3. Mechanical properties

As mentioned above, the two polymorphs exhibit very distinct mechanical properties. Specifically, upon application of external mechanical stress, the α phase undergoes elastic deformation and the β phase tends to plastically deform with development of defects and delamination (Figure SI11). Face indexing of both forms (SI, Figures SI8 and SI10) revealed that crystals of the α phase can be bent if subjected to a force perpendicular to their (001) face, while crystals of the β phase can be readily deformed when mechanical stress is applied perpendicular to their (100) face (Figure 9). The plastic behaviour of the β form can be ascribed to the presence of van der Waals interactions between the layers of C4-NT3N which involve the (100) slip planes, in fact, the energy framework indicates interaction energies on the (100) slip plane that range between -0.6 and -3.8 kJ/mol. Application of mechanical force on (100) causes slippage of adjacent layers, resulting in irreversible plastic deformation of the crystal (Figure 9c and SI, Figure SI11) while when the mechanical force is applied to different faces the crystal is fragile and brittle. For the α phase, the dispersive forces between the C4-NT3N columns are stronger, as it is apparent from the energy framework calculations, and prevent the slippage of π-stacked columns, allowing a reversible deformation of the lattice once an external force is applied perpendicular to the (001) face (Figure 9d).
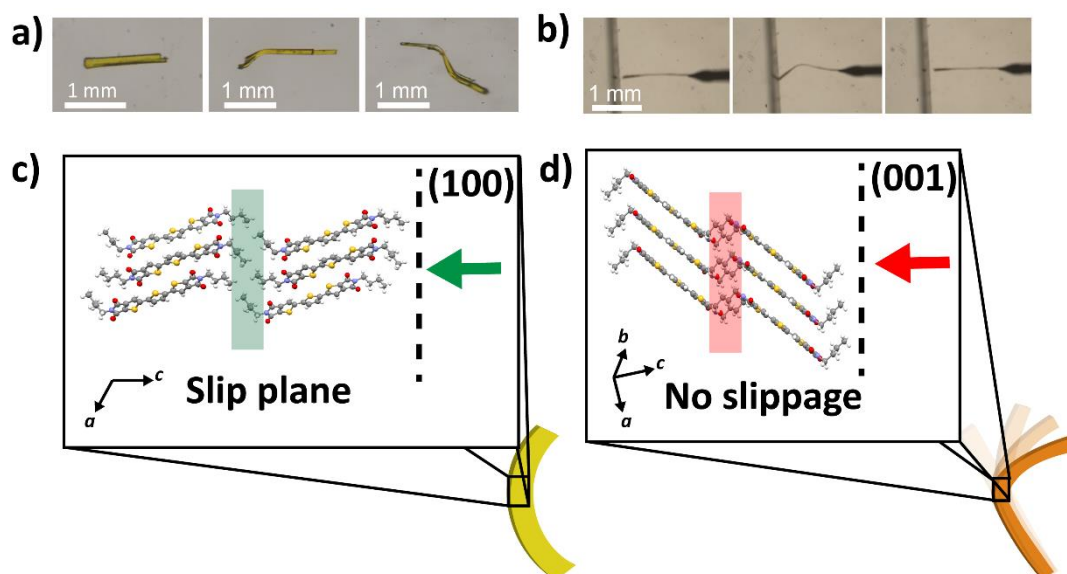
Figure 9. Representative crystals of both polymorphs of C4-NT3N showing elastic and plastic deformation. (a) From left to right, one straight crystal and two plastically deformed crystals of β phase; (b) From left to right, an α phase crystal is deformed and it readily recovers its original shape after the external force has been removed; (c) C4-NT3N columns in the structure of the β form viewed along the *b* axis with the slip plane responsible of the plastic behaviour highlighted in green and parallel to the (100) face of the crystal; (d) C4-NT3N columns in the structure of α form with the hindered plane responsible for the elastic behaviour highlighted in red and parallel to the (001) face of the crystal.

Nanoindentation measurements were performed to quantify the mechanical properties of the two crystalline phases.[40] The difference in mechanical behaviour was further confirmed at microscale *via* Atomic Force Microscopy (AFM) nanoindentation. The crystals were indented perpendicular to the (100) face for the β phase and to the (001) face of the α phase to obtain the respective Young's moduli (*E*) (for details, see the figure SI12). Surprisingly, an exceptional difference of one order of magnitude was found between the elastic moduli of the β form (*E* = 13 ± 3 MPa) and the α form (*E* = 147 ± 30

MPa), with the α form being stiffer than the β one. This result confirms that differences in crystal packing can have a profound impact on the mechanical properties of molecular crystalline materials. This result demonstrates for the first time difference in mechanical properties of an organic semiconductor by taking advantage of polymorphism.

2.4. Electronic and Optoelectronic Properties

As it can be expectable from the different packing features, the two polymorphs showed different electronic and optical properties. The energy band gap (E_g) of crystalline C4-NT3N is largely dependent on the molecular arrangement within the crystal lattice of the two phases. From reflectivity measurements, we were able to obtain the E_g of both polymorphs. In particular, the α phase has $E_g =$ 2.10 eV and the β phase has E_g = 2.29 eV (Figure 10). The photoluminescence spectra showed different emission maxima and lifetimes, confirming the results recently reported by some of the authors of the present work (see Experimental Section 4.8 and SI, Figure SI13).
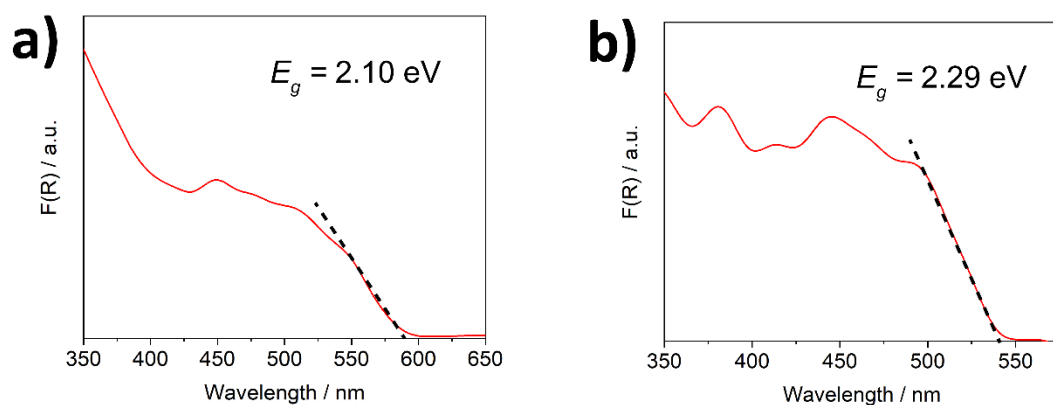

Figure 10. (a) Reflectivity spectrum of α phase, and the extrapolated E_g. (b) Reflectivity spectrum of β phase, and the extrapolated E_g.

To determine the electrical performance of both crystalline phases, capacitance-voltage (C–V) measurements were carried out on representative crystals of β and α forms (as specified in the Experimental Section 4.9). The C–V curves provide direct information on the electric field inside the crystals, which is strongly dependent on the variation of the charge carriers response in both polymorphs and their packing features. From the C–V measurements, we were able to obtain insights into the dielectric constants of both systems as function of frequency in the range 1 kHz – 2 MHz by using the following equation:

$$\varepsilon_1 = \frac{Y^*}{j\omega C_0} = \frac{C}{C_0} - i\frac{G}{\omega C_0}$$

where C and G are the measured capacitance and conductance of the dielectric material, Y^* the admittance and ω is the angular frequency ($\omega = 2\pi f$) of the applied electric field. The real part of the complex permittivity, the dielectric constant (ε), at various frequencies was calculated using the measured capacitance values under 25 V bias voltage as follow:

$$\varepsilon = \frac{C}{C_0} = \frac{Cd}{A\varepsilon_0}$$

where, d and A are the measured crystals thickness and area, respectively, and ε_0 (8.85×10^{-12} F/m) is the permittivity of vacuum. The calculated values of ε (reflecting how easily the crystal can be polarized by applying an electric field of 25 V/d) were found to be in the range of 116-100 and 106-94 for the β and the α polymorphs, respectively. High dielectric values were obtained at low frequencies in both crystal forms. This result can be explained as follows: at low frequencies, the four

types of polarization processes, i.e. the electronic, ionic, dipolar and interfacial and surface polarization, contribute to the magnitude of ε. On the other hand, at high frequencies, the contributions of the interfacial, dipolar and the ionic polarization become ineffective, leaving behind only the electronic part. This is due to the fact that at high frequencies, the interfacial dipoles have less time to orient themselves in the direction of the alternating field, which ultimately results in low dielectric values in both crystals.

3. CONCLUSIONS

The crystal structures of C4-NT3N in its α and β phases were determined, and the crystal packing allowed understanding of the remarkably different mechanical behaviour. The α form is characterized by 1D strong interactions due to the presence of π—π interactions. The weak hydrogen bonds and chalcogen bonds between the columns prevent their slippage, while allowing a reversible deformation of the lattice when an external force is applied perpendicular to the (001) face of the crystal. On the other hand, the β form presents 2D layer packing parallel to (001) with very weak interlayer interactions and without interdigitation of the alkyl chains. When force is applied perpendicular to the slip plane, plastic deformation occurs. The results of the nanoindentation measurements are consistent with the mechanical behaviour, with the α phase Young's modulus (E) being one order of magnitude higher than that of the β one ($E = 147 \pm 30$ MPa and $E = 13 \pm 3$ MPa, respectively). Since the electrical performances of the two polymorphs are comparable, the crystal form which should be implemented in the devices should be selected while considering the mechanical behaviour, and elastic crystals are preferred in case of bendable supports.

4. EXPERIMENTAL SECTION

4.1. Crystallization

C4-NT3N was synthesised following a procedure described in a previous aricle.[30] Precipitation of C4-NT3N in toluene as described in the synthetic protocol affords the β phase. The original powder was used for subsequent experiments without further purifications. The α phase can be obtained by solvent evaporation from a C4-NT3N solution (in CH_2Cl_2, CH_3Cl, toluene, xylene, THF). The β phase can be obtained inside a solvothermic reactor where a toluene solution of C4-NT3N is heated to a temperature of 120 °C and then slowly cooled down to the room temperature.

4.2. Single-crystal X-ray diffraction

Single crystal data were collected on an Oxford Xcalibur S instrument with MoK_α radiation (λ = 0.71073 Å) and graphite monochromator at room temperature. SHELXS[41] was used for structure solution and SHELXL[42] for the refinement based on F^2. The non-hydrogen atoms were refined anisotropically, and the hydrogen atoms were added at calculated positions. All crystallographic data and further details on the data collection and structure determination are reported in the Supporting Information. The software Mercury 4[43] was used to generate the molecular packing representation and for calculation of the diffraction pattern from the crystal structures. Using the software CrystalExplorer[39] it was possible to estimate the magnitude of the interaction energies in the two crystal forms. The CE-HF/3-21G was chosen as model energy (see SI for further details). The experimental data were deposited within the Cambridge Crystallographic Data Centre. CCDC1950934 and 1950920 contain the supplementary crystallographic data for this paper. These data can be obtained free of charge from the Cambridge Crystallographic Data Centre via www.ccdc.cam.ac.uk/data_request/cif.

4.3. X-ray powder diffraction

The powder diffraction patterns were recorded on a PANalytical X'Pert PRO diffractometer in Bragg-Brentano configuration equipped with a copper anode (CuK_α, λ = 1.5418 Å) and an X'Celerator Detector (Soller 0.04 rad, anti-scatter slit 1/8, divergence slit ¼, step size 0.017°). The synchrotron radiation XRPD measurements of C4-NT3N were performed at the Swiss Light Source (SLS) Material Science (MS) Powder Diffraction (PD) end station with a nominal photon energy of 16 keV. Fine Si640D NIST standard refinement returned a wavelength of 0.775375(2) Å and a residual zero error of −0.0253(4) 2θ, step size of 0,0036°. The measurements were performed in transmission geometry. The material was loaded inside a glass capillary with a diameter of 0.5 mm, spun at 4 Hz, and exposed to X-rays for 5 sec.

4.4. Hot-stage microscopy

The analysis was performed using a microscope OLYMPUS BX41 equipped with a VISICAM 5.0 and a NIKON DS FI3 camera. For the temperature control a Linkam TMS 94 stage was used. The photos were taken under polarised to underline the modification due to solid state transition, with a 40× and 100× magnification. Some photos were taken irradiating the crystals with a UV lamp at 365 nm in order to be able to observe differences in the emitted light.

4.5. Differential scanning calorimetry (DSC)

The analysis was performed with an instrument Perkin-Elmer PyrisDiamond DSC-7 equipped with a PII intracooler, in N_2 atmosphere and a scanning speed of 5°/min.

4.6. AFM nanoindentation

A commercial AFM (Keysight 5500, USA) was used to determine the mechanical properties of the crystal. Force modulation tip (Budget sensors model 75G, resonance frequency 75 kHz, spring constant 3 N m^{-1}) was used to perform the indentation experiments. The deflection sensitivity of the cantilever was estimated from the slope of the loading curve obtained on freshly cleaved mica, and the spring constant of the cantilever was calibrated according to the thermal tuning method. Force curves were acquired using the PicoView 1.20.2 software (Keysight Technologies) in the force volume mode, where a matrix of 16 ×16 forces curves were obtained on the crystal surface. Data analysis were performed using the SPIP software (Image Metrology, Denmark). Young's moduli of samples were estimated from fitting individual force-separation curves using the Johnson-Kendall-Roberts (JKR) model[36]. A nominal tip radius (20 nm) was used to estimate the mechanical properties from the force−distance profiles using the Johnson−Kendall−Roberts (JKR) modelling.

4.7. UV-visible spectroscopy

Solid-state UV-Vis spectra was acquired with Shimadzu NIR-Vis-UV 3600-UV spectrophotometer equipped with an ISR-3100 integrating sphere. Barium sulphate was used as a reference material and UV-Vis spectra were recorded in the range 300–800 nm.

4.8. Confocal microscopy

The confocal fluorescence measurements were performed on Leica TCS SP8 using a PicoQuant PDL 880-B 40 MHz pulsed 405 nm diode laser as excitation source. The fluorescence spectra were recorded with ±7 nm resolution. The measured lifetime of both polymorphs was uniformly distributed across the whole bent crystal with 1 ns lifetime for the α polymorph and 0.4 ns for the β polymorph.

4.9. Electrical characterization

The capacitance-voltage (C–V) measurements were carried out using an Agilent B 1505 A curve tracer at room temperature on single crystals of both polymorphs coated with silver paint (silver in isobutyl methyl ketone from Ted Pella Inc.) as electrical contacts.

BIBLIOGRAPHY

(1)   Bernstein, J. Crystal Growth, Polymorphism and Structure-Property Relationships in Organic Crystals. *J. Phys. D. Appl. Phys.* **1993**, *26* (8B), B66–B76. https://doi.org/10.1088/0022-3727/26/8B/010.

(2)   Bernstein, J. Polymorphism – A Perspective. *Cryst. Growth Des.* **2011**, *11* (3), 632–650. https://doi.org/10.1021/cg1013335.

(3)   Cruz-Cabeza, A. J.; Bernstein, J. Conformational Polymorphism. *Chem. Rev.* **2014**, *114* (4), 2170–2191. https://doi.org/10.1021/cr400249d.

(4)   Bernstein, J. *Polymorphism in Molecular Crystals*; Oxford University Press, 2007. https://doi.org/10.1093/acprof:oso/9780199236565.001.0001.

(5)   Gentili, D.; Gazzano, M.; Melucci, M.; Jones, D.; Cavallini, M. Polymorphism as an Additional Functionality of Materials for Technological Applications at Surfaces and Interfaces. *Chemical Society*

Reviews. May 7, 2019, pp 2502–2517. https://doi.org/10.1039/c8cs00283e.

(6)   Liu, D.; Li, C.; Niu, S.; Li, Y.; Hu, M.; Li, Q.; Zhu, W.; Zhang, X.; Dong, H.; Hu, W. A Case Study of Tuning

the Crystal Polymorphs of Organic Semiconductors towards Simultaneously Improved Light Emission

and Field-Effect Properties. *J. Mater. Chem. C* **2019**, *7* (20), 5925–5930.

https://doi.org/10.1039/c9tc01321k.

(7)   Boyle, C. J.; Upadhyaya, M.; Wang, P.; Renna, L. A.; Lu-Díaz, M.; Pyo Jeong, S.; Hight-Huf, N.; Korugic-

Karasz, L.; Barnes, M. D.; Aksamija, Z.; et al. Tuning Charge Transport Dynamics via Clustering of

Doping in Organic Semiconductor Thin Films. *Nat. Commun.* **2019**, *10* (1).

https://doi.org/10.1038/s41467-019-10567-5.

(8)   Abtahi, A.; Mazza, S. M.; Ryno, S. M.; Loya, E. K.; Li, R.; Parkin, S. R.; Risko, C.; Anthony, J. E.; Graham,

K. R. Effect of Halogenation on the Energetics of Pure and Mixed Phases in Model Organic

Semiconductors Composed of Anthradithiophene Derivatives and C $_{60}$. *J. Phys. Chem. C* **2018**, *122*

(9), 4757–4767. https://doi.org/10.1021/acs.jpcc.7b11729.

(9)   Ai, Q.; Jarolimek, K.; Mazza, S.; Anthony, J. E.; Risko, C. Delimited Polyacenes: Edge Topology as a

Tool To Modulate Carbon Nanoribbon Structure, Conjugation, and Mobility. *Chem. Mater.* **2018**, *30*

(3), 947–957. https://doi.org/10.1021/acs.chemmater.7b04715.

(10)   Li, D.; Wang, X.; Lin, Z.; Zheng, Y.; Jiang, Q.; Zheng, N.; Zhang, W.; Jin, K.; Yu, G. Tuning Charge Carrier

and Spin Transport Properties via Structural Modification of Polymer Semiconductors. *ACS Appl.*

Mater. Interfaces **2019**, *11* (33), 30089–30097. https://doi.org/10.1021/acsami.9b07863.

(11)   Phan, H.; Kelly, T. J.; Zhugayevych, A.; Bazan, G. C.; Nguyen, T.-Q.; Jarvis, E. A.; Tretiak, S. Tuning

Optical Properties of Conjugated Molecules by Lewis Acids: Insights from Electronic Structure

Modeling. *J. Phys. Chem. Lett.* **2019**, *10* (16), 4632–4638.

https://doi.org/10.1021/acs.jpclett.9b01572.

(12)   Maderitsch, A.; Pflumm, C.; Buchholz, H.; Borchert, H.; Parisi, J. The Impact of the Deposition Process

of the Emitting Layer on the Internal Structure of Organic Light-Emitting Diodes. *J. Phys. D. Appl.*

Phys. **2019**, *52* (45), 455105. https://doi.org/10.1088/1361-6463/ab375a.

(13)   Hiszpanski, A. M.; Baur, R. M.; Kim, B.; Tremblay, N. J.; Nuckolls, C.; Woll, A. R.; Loo, Y.-L. Tuning

Polymorphism and Orientation in Organic Semiconductor Thin Films via Post-Deposition Processing.

J. Am. Chem. Soc. **2014**, *136* (44), 15749–15756. https://doi.org/10.1021/ja5091035.

(14)   Minari, T.; Liu, C.; Kano, M.; Tsukagoshi, K. Controlled Self-Assembly of Organic Semiconductors for

Solution-Based Fabrication of Organic Field-Effect Transistors. *Adv. Mater.* **2012**, *24* (2), 299–306.

https://doi.org/10.1002/adma.201102554.

(15)   Galindo, S.; Tamayo, A.; Leonardi, F.; Mas-Torrent, M. Control of Polymorphism and Morphology in

Solution Sheared Organic Field-Effect Transistors. *Adv. Funct. Mater.* **2017**, *27* (25), 1700526.

https://doi.org/10.1002/adfm.201700526.

(16)   Khalifa, M.; Mahendran, A.; Anandhan, S. Probing the Synergism of Halloysite Nanotubes and

Electrospinning on Crystallinity, Polymorphism and Piezoelectric Performance of Poly(Vinylidene

Fluoride). *RSC Adv.* **2016**, *6* (115), 114052–114060. https://doi.org/10.1039/C6RA20599B.

(17)   Moazeni, N.; Latifi, M.; Merati, A. A.; Rouhani, S. Crystal Polymorphism in Polydiacetylene-

Embedded Electrospun Polyvinylidene Fluoride Nanofibers. *Soft Matter* **2017**, *13* (44), 8178–8187.

https://doi.org/10.1039/C7SM01252G.

(18)   Liu, D.; Li, C.; Niu, S.; Li, Y.; Hu, M.; Li, Q.; Zhu, W.; Zhang, X.; Dong, H.; Hu, W. A Case Study of Tuning

the Crystal Polymorphs of Organic Semiconductors towards Simultaneously Improved Light Emission

and Field-Effect Properties. *J. Mater. Chem. C* **2019**, *7* (20), 5925–5930.

https://doi.org/10.1039/C9TC01321K.

(19)   Benvenuti, E.; Gentili, D.; Chiarella, F.; Portone, A.; Barra, M.; Cecchini, M.; Cappuccino, C.;

         Zambianchi, M.; Lopez, S. G.; Salzillo, T.; et al. Tuning Polymorphism in 2,3-Thienoimide Capped

         Oligothiophene Based Field-Effect Transistors by Implementing Vacuum and Solution Deposition

         Methods. *J. Mater. Chem. C* **2018**, *6* (21), 5601–5608. https://doi.org/10.1039/C8TC00544C.

(20)   Hayashi, S.; Yamamoto, S. ya; Takeuchi, D.; Ie, Y.; Takagi, K. Creating Elastic Organic Crystals of π-

         Conjugated Molecules with Bending Mechanofluorochromism and Flexible Optical Waveguide.

         Angew. Chemie - Int. Ed. **2018**, *57* (52), 17002–17008. https://doi.org/10.1002/anie.201810422.

(21)   Hayashi, S.; Koizumi, T.; Kamiya, N. Elastic Bending Flexibility of a Fluorescent Organic Single Crystal:

         New Aspects of the Commonly Used Building Block 4, 7-Dibromo-2, 1, 3-Benzothiadiazole. *Cryst.*

         Growth Des. **2017**, *17* (12), 6158–6162. https://doi.org/10.1021/acs.cgd.7b00992.

(22)   Hayashi, S.; Koizumi, T. Elastic Organic Crystals of a Fluorescent π-Conjugated Molecule. *Angew.*

         Chemie - Int. Ed. **2016**, *55* (8), 2701–2704. https://doi.org/10.1002/anie.201509319.

(23)   Reddy, C. M.; Kirchner, M. T.; Gundakaram, R. C.; Padmanabhan, K. A.; Desiraju, G. R.

         Isostructurality, Polymorphism and Mechanical Properties of Some Hexahalogenated Benzenes: The

         Nature of Halogen···halogen Interactions. *Chem. - A Eur. J.* **2006**, *12* (8), 2222–2234.

         https://doi.org/10.1002/chem.200500983.

(24)   Wang, K.; Mishra, M. K.; Sun, C. C. Exceptionally Elastic Single-Component Pharmaceutical Crystals.

         Chem. Mater. **2019**, *31* (5), 1794–1799. https://doi.org/10.1021/acs.chemmater.9b00040.

(25)   Devarapalli, R.; Kadambi, S. B.; Chen, C. T.; Krishna, G. R.; Kammari, B. R.; Buehler, M. J.; Ramamurty,

         U.; Malla Reddy, C. Remarkably Distinct Mechanical Flexibility in Three Structurally Similar

         Semiconducting Organic Crystals Studied by Nanoindentation and Molecular Dynamics. *Chem.*

Mater. **2019**, *31* (4), 1391–1402. https://doi.org/10.1021/acs.chemmater.8b04800.

(26)   Saha, S.; Desiraju, G. R. Trimorphs of 4-Bromophenyl 4-Bromobenzoate. Elastic, Brittle, Plastic.
       Chem. Commun. **2018**, *54* (49), 6348–6351. https://doi.org/10.1039/c8cc02662a.

(27)   Kazantsev, M. S.; Konstantinov, V. G.; Dominskiy, D. I.; Bruevich, V. V.; Postnikov, V. A.; Luponosov,
       Y. N.; Tafeenko, V. A.; Surin, N. M.; Ponomarenko, S. A.; Paraschuk, D. Y. Highly Bendable
       Luminescent Semiconducting Organic Single Crystal. *Synth. Met.* **2017**, *232*, 60–65.
       https://doi.org/10.1016/j.synthmet.2017.07.019.

(28)   Durso, M.; Gentili, D.; Bettini, C.; Zanelli, A.; Cavallini, M.; De Angelis, F.; Grazia Lobello, M.; Biondo,
       V.; Muccini, M.; Capelli, R.; et al. π-Core Tailoring for New High Performance Thieno(Bis)Imide Based
       n-Type Molecular Semiconductors. *Chem. Commun. (Camb).* **2013**, *49* (39), 4298–4300.
       https://doi.org/10.1039/c2cc37053k.

(29)   Melucci, M.; Favaretto, L.; Zambianchi, M.; Durso, M.; Gazzano, M.; Zanelli, A.; Monari, M.; Lobello,
       M. G.; De Angelis, F.; Biondo, V.; et al. Molecular Tailoring of New Thieno(Bis)Imide-Based
       Semiconductors for Single Layer Ambipolar Light Emitting Transistors. *Chem. Mater.* **2013**, *25* (5),
       668–676. https://doi.org/10.1021/cm303224a.

(30)   Durso, M.; Bettini, C.; Zanelli, A.; Gazzano, M.; Lobello, M. G.; De Angelis, F.; Biondo, V.; Gentili, D.;
       Capelli, R.; Cavallini, M.; et al. Synthesis, Size-Dependent Optoelectronic and Charge Transport
       Properties of Thieno(Bis)Imide End-Substituted Molecular Semiconductors. *Org. Electron. physics,*
       Mater. Appl. **2013**, *14* (11), 3089–3097. https://doi.org/10.1016/j.orgel.2013.07.019.

(31)   Zambianchi, M.; Favaretto, L.; Durso, M.; Bettini, C.; Zanelli, A.; Manet, I.; Gazzano, M.; Maini, L.;
       Gentili, D.; Toffanin, S.; et al. Synergic Effect of Unsaturated Inner Bridges and Polymorphism for
       Tuning the Optoelectronic Properties of 2,3-Thieno(Bis)Imide Based Materials. *J. Mater. Chem. C*

2015, *3* (1), 121–131. https://doi.org/10.1039/C4TC01792G.

(32)   Melucci, M.; Zambianchi, M.; Favaretto, L.; Gazzano, M.; Zanelli, A.; Monari, M.; Capelli, R.; Troisi, S.;

Toffanin, S.; Muccini, M. Thienopyrrolyl Dione End-Capped Oligothiophene Ambipolar

Semiconductors for Thin Film- and Light Emitting Transistors. *Chem. Commun.* **2011**, *47* (43), 11840–

11842. https://doi.org/10.1039/c1cc14179a.

(33)   Maini, L.; Gallino, F.; Zambianchi, M.; Durso, M.; Gazzano, M.; Rubini, K.; Gentili, D.; Manet, I.;

Muccini, M.; Toffanin, S.; et al. Chemical Design Enables the Control of Conformational

Polymorphism in Functional 2,3-Thieno(Bis)Imide-Ended Materials. *Chem. Commun.* **2015**, *51* (11),

2033–2035. https://doi.org/10.1039/c4cc09177a.

(34)   Cappuccino, C.; Canola, S.; Montanari, G.; Lopez, S. G.; Toffanin, S.; Melucci, M.; Negri, F.; Maini, L.

One Molecule, Four Colors: Discovering the Polymorphs of a Thieno(Bis)Imide Oligomer. *Cryst.

Growth Des.* **2019**, *19* (5), 2594–2603. https://doi.org/10.1021/acs.cgd.8b01712.

(35)   Gentili, D.; Durso, M.; Bettini, C.; Manet, I.; Gazzano, M.; Capelli, R.; Muccini, M.; Melucci, M.;

Cavallini, M. A Time-Temperature Integrator Based on Fluorescent and Polymorphic Compounds.

Sci. Rep. **2013**, *3*, 2581. https://doi.org/10.1038/srep02581.

(36)   Johnson, K. L.; Kendall, K.; Roberts, A. D. Surface Energy and the Contact of Elastic Solids. *Proc. R.

Soc. A Math. Phys. Eng. Sci.* **1971**, *324* (1558), 301–313. https://doi.org/10.1098/rspa.1971.0141.

(37)   Mackenzie, C. F.; Spackman, P. R.; Jayatilaka, D.; Spackman, M. A. CrystalExplorer Model Energies

and Energy Frameworks: Extension to Metal Coordination Compounds, Organic Salts, Solvates and

Open-Shell Systems. *IUCrJ* **2017**, *4*, 575–587. https://doi.org/10.1107/S205225251700848X.

(38)   Turner, M. J.; Thomas, S. P.; Shi, M. W.; Jayatilaka, D.; Spackman, M. A. Energy Frameworks: Insights

into Interaction Anisotropy and the Mechanical Properties of Molecular Crystals. *Chem. Commun.*

2015, *51* (18), 3735–3738. https://doi.org/10.1039/c4cc09074h.

(39)   Turner M. J.; McKinnon J. J.; Wolff S. K.; Grimwood, D. J.; Spackman P. R.; Jayatilaka D.; Spackman M. A. CrystalExplorer17. 2017.

(40)   Varughese, S.; Kiran, M. S. R. N.; Ramamurty, U.; Desiraju, G. R. Nanoindentation in Crystal Engineering: Quantifying Mechanical Properties of Molecular Crystals. *Angewandte Chemie - International Edition*. 2013, pp 2701–2712. https://doi.org/10.1002/anie.201205002.

(41)   Sheldrick, G. M. SHELXT - Integrated Space-Group and Crystal-Structure Determination. *Acta Crystallogr. Sect. A Found. Crystallogr.* **2015**, *71* (1), 3–8. https://doi.org/10.1107/S2053273314026370.

(42)   Sheldrick, G. M. Crystal Structure Refinement with SHELXL. *Acta Crystallogr. Sect. C Struct. Chem.* **2015**, *71* (1), 3–8. https://doi.org/10.1107/S2053229614024218.

(43)   Macrae, C. F.; Bruno, I. J.; Chisholm, J. A.; Edgington, P. R.; McCabe, P.; Pidcock, E.; Rodriguez-Monge, L.; Taylor, R.; van de Streek, J.; Wood, P. A. Mercury CSD 2.0 – New Features for the Visualization and Investigation of Crystal Structures. *J. Appl. Crystallogr.* **2008**, *41* (2), 466–470. https://doi.org/10.1107/S0021889807067908.